Published in IET Communications
Received on 20th January 2014
Revised on 10th April 2014
Accepted on 25th April 2014
doi: 10.1049/iet-com.2014.0083

ISSN 1751-8628

Information theoretical performance limits of single-carrier underwater acoustic systems

Hatef Nouri[1], Murat Uysal[1], Erdal Panayirci[2], Habib Senol[2]

[1]*Department of Electrical and Electronics Engineering, Ozyegin University, Istanbul 34794, Turkey*
[2]*Department of Electrical and Electronics Engineering, Kadir Has University, Istanbul 34083, Turkey*
E-mail: hatef.nouri@ozu.edu.tr

Abstract: In this study, the authors investigate the information theoretical limits on the performance of point-to-point single-carrier acoustic systems over frequency-selective underwater channels with intersymbol interference. Under the assumptions of sparse and frequency-selective Rician fading channel and non-white correlated Gaussian ambient noise, the authors derive an expression for channel capacity and demonstrate the dependency on channel parameters such as the number, location and power delay profile of significant taps, as well as environmental parameters such as distance, temperature, salinity, pressure and depth. Then, the authors use this expression to determine the optimal carrier frequency, input signalling and bandwidth for capacity maximisation.

1 Introduction

Demands for underwater communication systems are increasing because of the on-going expansion of human activities in underwater environments such as scientific data collection, maritime archaeology, offshore oil field exploration/monitoring, port security, environmental monitoring and pollution control/tracking among others [1–9]. For example, maritime archaeology [1, 2] studies the past of human life, behaviours and cultures and their activities in, on, around and under the sea. Its acceptance has been a relatively late development because of the difficulties of accessing and working in underwater sites. This branch of science can benefit significantly from effective use of underwater communication systems. Furthermore, the vast underwater world is extremely rich in natural resources such as valuable minerals and oil fields waiting to be explored. Seismic monitoring [3–5] becomes particularly important in oil extraction from underwater fields to assess the field performance. In addition, monitoring the oil rigs can help taking preventive actions for the disasters such as the rig explosion that took place in the Gulf of Mexico in 2010 [6, 7]. Tsunami and earthquake forewarning [3, 8] systems can benefit from seismic information which is measured from undersea locations and also such collected information can be used in studies of the seaquakes. Last, but not least, there are a large number of underwater military applications [9] which include surveillance, submarine detection, mine reconnaissance missions and unmanned operations.

The current typical choice for oceanographic data acquisition is to deploy underwater sensors which record data during the monitoring mission and then recover the information from the storage unit of sensor [3, 5, 6, 8]. Such an off-line approach is not able to deliver real-time information which can be particularly critical in surveillance and disaster prevention. There is also an increasing use of robotics in underwater missions in order to increase precision and operability [3, 4, 9]. Remotely operated vehicles (ROVs) and autonomous underwater vehicles (AUVs) are usually used in such applications and an important point is how to communicate with the ROV or AUV. Classically, cabled or fibre-based techniques are used. Although these approaches provide high-speed and reliable communication, their use can be challenging in difficult-access locations and in deep sea as they will limit the range and manoeuvrability of the ROV.

Such problems with wireline technologies trigger the demand for reliable high-speed underwater wireless links. Radio-frequency (RF) signals suffer from large attenuations in water and long-range RF communication requires the use of extra low frequencies which necessitate large antennas and high transmit powers [3]. Optical signals do not suffer much from attenuation, but absorption, scattering and high level of ambient light limit the transmission range to a few metres. Among the alternatives for wireless underwater communications, acoustic transmission is the most practical and commonly employed method [2]. The characteristics of underwater acoustic (UWA) channel, such as multipath fading, bandwidth limitations and sparsity still pose many challenges to the development of underwater systems [10]. For efficient UWA communication system design, it is important to understand the fundamental performance limits imposed by the underwater channels. From an information theoretic point of view, the basic performance measure is the capacity of a channel which determines the maximum data rate that can be supported with an arbitrarily small error probability.

Although capacity calculations for terrestrial wireless RF channels have been extensively studied, see for example [11], the literature on the capacity of UWA channels is sporadic [12–14] with many remaining open questions. To the best of our knowledge, the capacity of UWA channel has been first studied by Kwon and Birdsall [15]. However, they oversimplify the UWA channel model ignoring the multipath fading effects and use a time-invariant channel model with additive Gaussian noise that may or may not be white. The work in [16] assumes a Rayleigh fading model with additive white Gaussian noise (AWGN). In [17], achievable rates are derived for an orthogonal frequency division multiplexing (OFDM) system on highly dispersive channels assuming no channel state information (CSI) at transmitter and receiver. Numerical assessments of their derived expressions using experimental channel data show that OFDM transmissions at 2–4 bit/s/Hz are achievable at an average signal-to-noise ratio (SNR) of 15–20 dB.

None of the aforementioned works takes into account the path loss in signal models; therefore their results do not reflect the dependence of the capacity on distance. The path loss effects are further taken into account in [12–14]. These works, either implicitly [12] or explicitly [14] consider an OFDM-based multi-carrier architecture and assume frequency-flat channel for each narrow sub-band. In an OFDM system, assuming that there are enough parallel channels, the frequency-selective channel is effectively disintegrated into a number of frequency-flat channels and no intersymbol interference (ISI) is observed. Therefore the fading effect is modelled as a multiplicative coefficient.

On the other hand, single-carrier systems over frequency-selective channels are subject to ISI which needs to be taken into account in the performance analysis. In [13], Choudhuri and Mitra derive capacity bounds for the UWA relay channels with ISI and investigate optimum power allocation. They, however, consider some idealistic assumptions such as Thorp's formula [18] for the path loss which depends on only distance and frequency ignoring the effect of environmental parameters.

In this paper, we readdress the information theoretical limits of UWA channels with ISI. We assume non-white Gaussian to model the ambient noise [19] and consider Francois–Garrison formula [20, 21] to take into account the effects of environmental parameters such as temperature, salinity, pressure, depth as well as distance and frequency. Exploiting the methodology introduced in [22], we develop an equivalent channel model for UWA channel with ISI and show that the capacity of the equivalent channel converges to that of the operating channel in the limit of infinite block length. Using these results, we first obtain a capacity expression for the UWA channel under consideration and demonstrate the dependency on channel parameters such as the number, location and power delay profile (PDP) of significant taps, as well as environmental parameters such as temperature, salinity, pressure and depth. Then, we use this expression to determine the optimal carrier frequency, input signalling and bandwidth.

The rest of this paper is summarised as follows: in Section 2, we describe the UWA channel model including path loss, fading and ambient noise. In Section 3, we introduce our transmission model. In Section 4, we present the derivations of instantaneous and average channel capacity. In Section 5, we investigate the effect of channel parameters on the average capacity. In Section 6, we present numerical results to corroborate the analytical derivations. In Section 7, we discuss the optimal choice of carrier frequency, input signalling and bandwidth for performance optimisation. In Section 8, we finally conclude this paper.

Notation: $(.)^{\mathrm{T}}$, $(.)^*$ denote transpose and complex conjugate-transpose operations, respectively. $E(.)$ denotes statistical expectation and $|.|$ denotes determinant. $*$ and $\otimes$ denote linear and circular convolutions. $[x]^+$ is equivalent to $\max\{0, x\}$. $\mathbb{R}$ denotes real numbers and $\mathbb{Z}_0$ denotes set of integers. Bold upper-case and lower-case letters denote matrices and vectors, respectively. $R_x[l] = E(x[k+l-1]x[k])$, $l \in \{1, 2, \ldots, N\}$ denotes the autocorrelation function of discrete signal $x[k]$, $k \in \{1, 2, \ldots, N\}$. $x[k] \overset{F}{\longleftrightarrow} x(f_n)$ denotes the discrete Fourier transform (DFT) of the discrete signal $x[k]$ which are the samples of the function $x(t)$. Here, $x(f_n) = \sum_{k=1}^{N} x[k]\mathrm{e}^{-\mathrm{j}2\pi(k-1)f_n}\Delta f$, $n \in \{1, 2, \ldots, N\}$, $\Delta f = 1/N$ and $f_n = (n-1)\Delta f$. $\boldsymbol{F}$ is defined as the DFT matrix with elements $\boldsymbol{F}(k, n) = (1/\sqrt{N})\exp(-\mathrm{j}2\pi(k-1)(n-1)/N)$ and $\forall k, n \in \{1, 2, \ldots, N\}$.

2 UWA channel model

In this chapter, we describe the large-scale path loss, small-scale fading and coloured Gaussian noise models of UWA channels.

2.1 Path loss

The large-scale UWA path loss is given by $A(f, d) = d^s a(f)^d$ where d is the distance between the transmitter and receiver, $1 \le s \le 2$ is the spreading factor and $a(f)$ is the absorption coefficient. According to Francois–Garrison formula [20, 21], the absorption coefficient is expressed as

$$a(f) = \frac{A_1 B_1 C_1 f^2}{C_1^2 + f^2} + \frac{A_2 B_2 C_2 f^2}{C_2^2 + f^2} + A_3 B_3 f^2 \ \mathrm{dB/km} \quad (1)$$

where f is the carrier frequency (in kHz), A_i, $i = 1, 2, 3$ are the temperature and salinity dependencies, B_i, $i = 1, 2, 3$ are the pressure dependencies and C_i, $i = 1, 2, 3$ are the relaxation frequencies.

2.2 Ambient noise

There are four main sources of ambient noise (turbulence, shipping, waves and thermal noise) each of which becomes dominant in different frequency regions. Considering that most practical UWA systems operate in the frequency range of 10–100 kHz, waves' noise becomes the dominating factor. Power spectral density (PSD) for waves' noise (in dB re 1 μPa/Hz) is given by [19]

$$10 \log Z_w(f) = 50 + 7.5\omega^{1/2} + 20 \log f - 40 \log (f + 0.4) \quad (2)$$

where ω is the wind speed. For a tractable mathematical model, this can be approximated by [23]

$$10 \log Z_w(f) = 50 + 7.5\omega^{1/2} - 10 \log (f^2 + f_0^2) \quad (3)$$

which can be rewritten as $Z_w(f) = f_0\sigma^2/(\pi f^2 + \pi f_0^2)$ where $\sigma^2 = E[z(t)z^*(t)] = (\pi 10^{5+0.75\sqrt{w}})/f_0$ and f_0 is the lowest cut-off frequency. The corresponding autocorrelation function can be then easily obtained by taking inverse

doi: 10.1049/iet-com.2014.0083

Fourier transform of $Z_w(f)$ and is given by

$$R_w(\tau) = \sigma^2 \exp(-2\pi f_0|\tau|), \quad \forall \tau \in \mathbb{R} \tag{4}$$

2.3 Fading model

The average received power is determined by the path loss, but instantaneous level of the received power fluctuates as a result of small-scale fading effects because of multipath propagation in underwater environments. The resulting frequency-selective sparse UWA channel can be modelled as a finite impulse response filter. Let $T \cong 1/W$ denote the sampling rate of the input symbols where W is the transmission bandwidth. Assume that T_d denotes the delay spread. The channel length is given by $L = \lceil T_d/T \rceil$. The impulse response of the channel is [24]

$$h[k,\ l] = \sum_{i=1}^{L} h_i[k]\delta[l-i] \tag{5}$$

where $h_i \overset{F}{\longleftrightarrow} h(f_n)$, $i \in \{1,\ 2,\ \ldots,\ L\}$ denote channel tap coefficients and the corresponding discrete channel frequency gains.

Although there is not a general consensus within the research community about the theoretical distribution for statistical characterisation of tap coefficients in underwater channels, the small-scale effects are often modelled as Rayleigh or Rician fading [25]. In this paper, we consider Rician fading which also includes Rayleigh fading as a special case. Under Rician fading assumption, h_i is modelled as a complex non-zero mean Gaussian random process with independent real and imaginary parts having a mean of $\mu_i/\sqrt{2}$ and a variance of σ_i^2. The power of the ith tap is therefore $\Omega_i = E(|h_i|^2) = \mu_i^2 + 2\sigma_i^2$ and the normalised total power is $\sum_i \Omega_i = 1$. The channel PDP vector is defined as $\boldsymbol{\Omega} = [\Omega_1,\ \Omega_2,\ \ldots,\ \Omega_L]$ with cardinality $|\boldsymbol{\Omega}| = L$. Since the UWA channel exhibits sparse characteristics, we further define vectors $\boldsymbol{\Psi}$ and $\boldsymbol{\Gamma}$ which, respectively, denote the PDP and the locations of only significant channel taps. Their cardinality is $|\boldsymbol{\Psi}| = |\boldsymbol{\Gamma}| = m$ where $m \ll L$ is the number of significant taps. Introducing the Rician factor as $k_i = \mu_i^2/2\sigma_i^2$, each channel tap can be written as

$$h_i = \sqrt{\frac{\Omega_i k_i}{k_i+1}}\left(\frac{1+j}{\sqrt{2}}\right) + \sqrt{\frac{\Omega_i}{k_i+1}}\alpha_i \tag{6}$$

where α_i is a complex Gaussian random variable with zero mean and unit variance.

3 Transmission model

Consider a transmission block size of N and let the discrete source signal be represented by $x[k]$, $k = 1,\ 2,\ \ldots,\ N$. The autocorrelation function and the corresponding discrete PSD of the input signal are $R_x[k] \overset{F}{\longleftrightarrow} P(f_n)$, $k \in \{1,\ 2,\ \ldots,\ N-1\}$. The autocorrelation matrix of the input signal is therefore defined by $\boldsymbol{R}_x = E(\boldsymbol{x}\boldsymbol{x}^*)$ where $\boldsymbol{x} = (x[1],\ x[2],\ \ldots,\ x[N])$. The power constraint is given by

$$\frac{1}{N}\sum_{k=1}^{N} E(|x[k]|^2) \le P_t \tag{7}$$

where NP_t is the maximum average energy allowed per block and expectation is with respect to the distributions of $x[k]$, $k = 1,\ 2,\ \ldots,\ N$, that is, $p(\boldsymbol{x}) = \prod_{i=1}^{N} p(x[i]|x[i-1])$. The received signal is given by

$$y[k] = h[k,\ l] * g[k] * x[k] + w[k], \quad k = 1,\ 2,\ \ldots,\ N \tag{8}$$

where $w[k]$ is the additive non-white Gaussian noise term with the autocorrelation function and the corresponding discrete PSD of $R_w[k] \overset{F}{\longleftrightarrow} Z_w(f_n)$, $k \in \{1,\ 2,\ \ldots,\ N-1\}$. Note that in the limit of $N \to \infty$, $Z_w(f_n)$ converges to $Z_w(f)$ in (2) by definition of DFT. The autocorrelation matrix of noise signal is defined as $\boldsymbol{R}_w = E(\boldsymbol{w}\boldsymbol{w}^*)$ based on the discrete version of autocorrelation function given by (4). In (8), $g[k] \overset{F}{\longleftrightarrow} g(f_n)$, $k \in \{1,\ 2,\ \ldots,\ N\}$ represents the effect of large-scale impairments and is the discrete version of function $g(t)$ whose PSD is given by $G(f,\ d) = 1/A(f,\ d)$ (compare Section 2.1). In discrete-time domain, it can be shown that the discretised version of the PSD, that is, $G(f_n,\ d)$ is equivalent to $|g(f_n)|^2$. Under the assumption that the channel remains constant over a transmission block and replacing (5) in (8), we have

$$y[k] = \sum_{i=1}^{L} h_i(g * x)[k-i] + w[k] \tag{9}$$

The channel in (9) is referred to as 'N-block discrete-time Gaussian channel (N-DTGC)' in [22]. In the following, we exploit a technique introduced in [22] which develops an 'equivalent hypothetical' circular channel model for the N-DTGC channel. This is named as 'N-block circular Gaussian channel (N-CGC)' and shown to have the same capacity with that of N-DTGC in the limit of infinite block length. In this equivalent model, the received signal is given by

$$\begin{aligned}\bar{y}[k] &= \sum_{i=1}^{L}\sum_{j=1}^{N} h_i g[j] x[(k-i-j)_N] + \bar{w}[k] \\ &= h[k,\ l] \otimes g[k] \otimes x[k] + \bar{w}[k]\end{aligned} \tag{10}$$

where the operator $(.)_N$ is defined as

$$(k)_N = \begin{cases} k - N\left\lfloor \dfrac{k}{N} \right\rfloor, & \text{if} \quad k \ne lN, \quad l \in \mathbb{Z}_0 \\ N, & \text{if} \quad k = lN, \quad l \in \mathbb{Z}_0 \end{cases} \tag{11}$$

In (10), $\bar{w}[k]$ is additive non-white Gaussian noise term with periodic autocorrelation function [26] given by $R_{\bar{w}}[k] = E(\bar{w}[k]\bar{w}[j]) \overset{F}{=} R_w[k-j] + R_w[k-j+N] + R_w[k-j-N]$ and $R_{\bar{w}}[k] \overset{F}{\longleftrightarrow} Z_{\bar{w}}(f_n)$, $k, j \in \{1,\ 2,\ \ldots,\ N\}$. Noting that it is a periodic repetition of R_w and noise samples from different blocks are independent, we have $R_{\bar{w}}[k] = R_w[k]$ and $Z_{\bar{w}}(f_n) = Z_w(f_n)$ for $\forall n \in \{1,\ 2,\ \ldots,\ N\}$.

The output sequence in vector form is given by

$$\bar{\boldsymbol{y}} = \boldsymbol{C}\boldsymbol{H}\boldsymbol{x} + \bar{\boldsymbol{w}} \tag{12}$$

where $\bar{\boldsymbol{y}} = (\bar{y}[1],\ \bar{y}[2],\ \ldots,\ \bar{y}[N])$ and $\bar{\boldsymbol{w}} = (\bar{w}[1],\ \bar{w}[2],\ \ldots,\ \bar{w}[N])$. In (12), $\boldsymbol{C}$ and $\boldsymbol{H}$ are circulant matrices with elements $[\boldsymbol{H}]_{i,j} = h_{(j-i+1)_N}$ and $[\boldsymbol{C}]_{i,j} = g[(j-i+1)_N]$. Note that circulant matrices can be diagonalised by DFT matrix

$\boldsymbol{F}$. Let us define $\bar{\boldsymbol{Y}} = \boldsymbol{F}\bar{\boldsymbol{y}}$, then we have

$$\bar{\boldsymbol{Y}} = \boldsymbol{GDX} + \bar{\boldsymbol{W}} \tag{13}$$

where $\boldsymbol{G} = \boldsymbol{FCF}^*$, $\boldsymbol{D} = \boldsymbol{FHF}^*$, $\boldsymbol{X} = \boldsymbol{Fx}$ and $\bar{\boldsymbol{W}} = \boldsymbol{F}\bar{\boldsymbol{w}}$. Note that $\boldsymbol{G}$ and $\boldsymbol{D}$ are diagonal matrices with diagonal elements $G_{nn} = \sum_{k=1}^{N} g[k]\mathrm{e}^{-\mathrm{j}2\pi(k-1)(n-1)/N}\Delta f$ and $D_{nn} = \sum_{i=1}^{L} h_i\mathrm{e}^{-\mathrm{j}2\pi(i-1)(n-1)/N}\Delta f$ or, equivalently, $G_{nn} = g(f_n)$ and $D_{nn} = h(f_n)$.

4 Capacity analysis

In this section, we first present the derivation of instantaneous channel capacity for a given realisation of the fading channel. Then, by performing an expectation over the fading distribution, we obtain average channel capacity.

4.1 Derivation of instantaneous channel capacity

The equivalent channel model N-CGC decomposes the multipath channel into a set of N parallel Gaussian channels via DFT decomposition. Considering the input–output relation in (13) and noting that the linear DFT operation does not affect the information rate of the channel, the capacity of N-CGC is given by

$$C_N^c = \sup_{p(\boldsymbol{x})} \frac{1}{N} I(\boldsymbol{X};\ \bar{\boldsymbol{Y}}) \tag{14}$$

The capacity of the N-DTGC under consideration can then be found by letting $N \to \infty$, that is

$$C = \lim_{N\to\infty} C_N^c = \lim_{N\to\infty} \sup_{p(\boldsymbol{x})} \frac{1}{N} I(\boldsymbol{X};\ \bar{\boldsymbol{Y}}) \tag{15}$$

where the maximisation is taken over the input distribution. The mutual information is given by

$$I(\boldsymbol{X};\ \bar{\boldsymbol{Y}}) = \mathcal{H}(\bar{\boldsymbol{Y}}) - \mathcal{H}(\bar{\boldsymbol{Y}}|\boldsymbol{X}) \tag{16}$$

where $\mathcal{H}(.)$ is differential entropy. Replacing (13) in (16), we have

$$\begin{aligned} I(\boldsymbol{X};\ \bar{\boldsymbol{Y}}) &= \mathcal{H}(\boldsymbol{GDX} + \bar{\boldsymbol{W}}) - \mathcal{H}(\bar{\boldsymbol{W}}) \\ &\le \frac{1}{2}\log 2\pi e\left|\boldsymbol{GDK}_{\boldsymbol{X}}\boldsymbol{D}^*\boldsymbol{G}^* + \boldsymbol{K}_{\bar{\boldsymbol{W}}}\right| - \frac{1}{2}\log 2\pi e\left|\boldsymbol{K}_{\bar{\boldsymbol{W}}}\right| \end{aligned} \tag{17}$$

where $\boldsymbol{K}_{\boldsymbol{X}} = E(\boldsymbol{XX}^*) = \boldsymbol{FR}_{\boldsymbol{x}}\boldsymbol{F}^*$ and $\boldsymbol{K}_{\bar{\boldsymbol{W}}} = E\left(\bar{\boldsymbol{W}}\bar{\boldsymbol{W}}^*\right) = \boldsymbol{FR}_{\bar{w}}\boldsymbol{F}^*$ are, respectively, the DFT of input and noise autocorrelation matrices. Owing to the periodic property of autocorrelation function $R_{\bar{w}}[k]$, the autocorrelation matrix $\boldsymbol{R}_{\bar{w}}$ is circulant. Hence, $\boldsymbol{R}_{\bar{w}}$ can be diagonalised by the DFT which results in the diagonality of $\boldsymbol{K}_{\bar{\boldsymbol{W}}}$. The inequality comes from the fact that Gaussian distribution of input maximises the entropy.

Hadamard's inequality [27] implies that diagonal $\boldsymbol{K}_{\boldsymbol{X}}$ maximises the mutual information. Therefore (16) is further upper bounded by

$$I(\boldsymbol{X};\ \bar{\boldsymbol{Y}}) \le \frac{1}{2}\sum_{n=1}^{N} \log\left(1 + \frac{|G_{nn}|^2|D_{nn}|^2 K_{Xnn}}{K_{\bar{W}nn}}\right) \tag{18}$$

where $K_{Xnn} = \sum_{k=1}^{N} R_x[k]\mathrm{e}^{-\mathrm{j}2\pi(k-1)(n-1)/N}\Delta f$ and $K_{\bar{W}nn} = \sum_{k=1}^{N} R_{\bar{w}}[k]\mathrm{e}^{-\mathrm{j}2\pi(k-1)(n-1)/N}\Delta f$ are the diagonal components of $\boldsymbol{K}_{\boldsymbol{X}}$ and $\boldsymbol{K}_{\bar{\boldsymbol{W}}}$ which correspond to the discrete values of input signal PSD and noise PSD, that is, $K_{Xnn} = P(f_n)$, $K_{\bar{W}nn} = Z_w(f_n)$. In (18), we replace $|G_{nn}|^2$ and $|D_{nn}|^2$ with $G(f_n,\ d)$ and $|h(f_n)|^2$, respectively. We can therefore rewrite the capacity as

$$\begin{aligned} C &= \lim_{N\to\infty} \max_{P(f_n)} \frac{1}{2N}\sum_{n=1}^{N} \log\left(1 + \frac{G(f_n,\ d)|h(f_n)|^2 P(f_n)}{Z_w(f_n)}\right) \\ &\text{subject to } \frac{1}{N}\sum_{n=1}^{N} P(f_n) \le P_t \end{aligned} \tag{19}$$

As the number of sub-bands N grows, the frequency width, that is, Δf, goes to zero in the limit of $N \to \infty$, and they represent a finer sampling of the continuous spectrum. Then (19) converges to

$$\begin{aligned} C &= \max_{P(f)} \frac{1}{2}\int_{-1/2}^{1/2} \log\left(1 + \frac{G(f,\ d)|h(f)|^2 P(f)}{Z_w(f)}\right) \mathrm{d}f \ \text{bit/s/Hz} \\ &\text{subject to } \int_{-1/2}^{1/2} P(f)\,\mathrm{d}f \le P_t \end{aligned} \tag{20}$$

Considering a specific bandwidth W, the capacity (in bit/s) can be found with the same procedure by replacing $\Delta f = W/N$ in the definition of DFT. Capacity in bit/s is therefore obtained as

$$\begin{aligned} C &= \max_{P(f)} \frac{1}{2}\int_{W} \log\left(1 + \mathrm{SNR}(f)\right) \mathrm{d}f \\ &\text{subject to } \frac{1}{W}\int_{W} P(f)\,\mathrm{d}f \le P_t \end{aligned} \tag{21}$$

Here, the integration is over the operating band and the narrowband SNR is defined as $\mathrm{SNR}(f) = G(f,d)|h(f)|^2P(f)/Z_w(f)$. It is worth mentioning that the above capacity expression also includes Gaussian channel with no ISI, that is, $|h(f)|^2 = 1$, and frequency-flat Rician fading channel, that is, $|h(f)|^2 = |h_1|^2$, as special cases.

4.2 Derivation of average channel capacity

The expression in (21) is provided for a given realisation of the channel. To find the average capacity, one needs to take expectation of (21) with respect to distribution of $|h(f)|^2$. $h(f)$ is the Fourier transform of the discrete channel taps, that is, $h(f) = \sum_{i=1}^{L} h_i\mathrm{e}^{-\mathrm{j}2\pi f(i-1)}$ where h_i's are complex Gaussian random processes with independent real and imaginary parts having a mean of $\mu_i/\sqrt{2}$ and a variance of σ_i^2 (compare Section 2.3). Since $h(f)$ is a linear summation of independent complex Gaussian random processes, it is also a complex Gaussian random process with mean $\mu(f) = \sum_{i=1}^{L} E(h_i)\mathrm{e}^{-\mathrm{j}2\pi f(i-1)}$ and variance $\sigma_h^2 = \sum_{i=1}^{L} 2\sigma_i^2$. Considering that $\sum_i\left(\mu_i^2 + 2\sigma_i^2\right) = 1$ (compare Section 2.3), it is easy to show that $|h(f)|^2$ follows the exponential pdf [28]

$$p(|h(f)|^2) = \frac{1}{1+\lambda}\exp\left(-\frac{|h(f)|^2}{1+\lambda}\right) \tag{22}$$

doi: 10.1049/iet-com.2014.0083

where λ is defined as

$$\lambda = 2\sum_{i=1}^{L}\sum_{j=i+1}^{L}\mu_i\mu_j\cos(2\pi f(j-i)) \tag{23}$$

Under the assumption that CSI is only available at the receiver side, the source allocates equal power across the sub-bands as it has no knowledge of the channel at the transmitter side. Setting $P(f) = P_t$ in (21), we need to calculate

$$\bar{C} = E_{|h(f)|^2}\left(\frac{1}{2}\int_W \log\left(1+\frac{G(f,d)P_t}{Z_w(f)}|h(f)|^2\right)\mathrm{d}f\right) \tag{24}$$

Assuming $\rho = |h(f)|^2/(1+\lambda)$, (24) can be written as

$$\bar{C} = \frac{1}{2}\int_W\int_0^\infty \log\left(1+\frac{(1+\lambda)G(f,d)P_t}{Z_w(f)}\rho\right)\exp(-\rho)\,\mathrm{d}\rho\,\mathrm{d}f \tag{25}$$

Using the results of [28], we can rewrite (25) as (see (26))

where $\Gamma(a,\ z) = \int_z^\infty t^{a-1}\mathrm{e}^{-t}\,\mathrm{d}t$ denotes the 'incomplementary gamma function'. Using the first series expansion of $\Gamma(0,\ z)$ [28, 29] and substituting it in (26) we have (see (27))

where γ is the Euler constant ($\gamma = 0.577215665$). At high SNR values (27) can be approximated as (see (28))

5 Effect of channel parameters on the average capacity

In this section, we investigate the effect of location of significant channel taps and PDP on the average capacity.

5.1 Location of significant taps

Note that the term λ defined in (23) contains all the information about PDP and location of significant taps. It can be readily verified that we will have $\lambda = 0$ for a frequency-flat channel. Considering the average capacity expression in (27), we observe that the term $1+\lambda$ is multiplied to the transmit power, meaning that PDP and taps' location will affect the received power through this term. Therefore in order to quantify the effect of PDP and taps' location on the capacity, we investigate the behaviour of the term $1+\lambda$.

Recall from Section 2.3 that $\boldsymbol{\Gamma} = [\Gamma_1, \Gamma_2, \ldots, \Gamma_m]$ defines the location vector of significant taps. Therefore we can rewrite (23) as

$$1+\lambda = 1+2\sum_{i=1}^{m}\sum_{j=i+1}^{m}\mu_{\Gamma_i}\mu_{\Gamma_j}\cos(2\pi f(\Gamma_j-\Gamma_i)) \tag{29}$$

After some mathematical manipulations, we obtain

$$\begin{aligned}1+\lambda = \frac{1}{1+k} &+ \left(\sum_{i=1}^{m}\mu_{\Gamma_i}\cos(2\pi\Gamma_i f)\right)^2 \\ &+ \left(\sum_{i=1}^{m}\mu_{\Gamma_i}\sin(2\pi\Gamma_i f)\right)^2\end{aligned} \tag{30}$$

where k is the Rician factor. Using Cauchy–Schwarz inequality, we can find bounds on $1+\lambda$ as

$$\frac{1}{1+k} \le 1+\lambda \le \frac{1+mk}{1+k} \tag{31}$$

In the rest of this section, we assume uniform PDP (i.e. $\Omega_i = 1/m$). Consequently we can write

$$\mu_i = \sqrt{\frac{k}{m(1+k)}},\ \text{for}\ \forall i \tag{32}$$

Under the assumption that difference between the locations of two consequence channel taps is constant and equal to r (i.e. $\Gamma_{i+1} - \Gamma_i = r$, for $\forall i$), we can rewrite (30) as

$$1+\lambda = \frac{1}{k+1} + \left(\frac{k}{m(k+1)}\right)\frac{1-\cos(m2\pi rf)}{1-\cos(2\pi rf)} \tag{33}$$

The minimum and maximum values of (33) are found as

$$\min\{1+\lambda\} = \frac{1}{k+1} \tag{34}$$

$$\max\{1+\lambda\} = \frac{1}{k+1} + \left(\frac{k}{m(k+1)}\right)\underbrace{\max\left\{\frac{1-\cos(m2\pi rf)}{1-\cos(2\pi rf)}\right\}}_{m^2} \tag{35}$$

The maximum value takes place when $1-\cos(2\pi rf) = 0$. For $0 \le f \le 1$, the solution is $f = i/r$, $i = 0,\ 1,\ 2,\ \ldots,\ r$ and the number of peaks is equal to $r+1$. As r increases, the number of peaks in $1+\lambda$ increases, therefore the capacity increases. As a conclusion, we can state that, under the assumption of uniform PDP, as the spacing between significant taps increases, capacity increases and becomes closer to the capacity of frequency-flat channel.

$$\bar{C} = \frac{\log_2(e)}{2}\int_W \exp\left(\frac{Z_w(f)}{(1+\lambda)G(f,d)P_t}\right)\Gamma\left(0,\ \frac{Z_w(f)}{(1+\lambda)G(f,d)P_t}\right)\mathrm{d}f \tag{26}$$

$$\bar{C} = \frac{\log_2(e)}{2}\int_W \exp\left(\frac{Z_w(f)}{(1+\lambda)G(f,d)P_t}\right)\left[-\gamma + \ln\left(\frac{(1+\lambda)G(f,d)P_t}{Z_w(f)}\right) - \sum_{k=1}^{\infty}\frac{1}{kk!}\left(\frac{-Z_w(f)}{(1+\lambda)G(f,d)P_t}\right)^k\right]\mathrm{d}f \tag{27}$$

$$\bar{C} \simeq \frac{\log_2(e)}{2}\int_W \exp\left(\frac{Z_w(f)}{(1+\lambda)G(f,d)P_t}\right)\left[-\gamma + \ln\left(\frac{(1+\lambda)G(f,d)P_t}{Z_w(f)}\right) + \frac{Z_w(f)}{(1+\lambda)G(f,d)P_t}\right]\mathrm{d}f \tag{28}$$

5.2 Effect of PDP

The PDP vector of significant taps $\boldsymbol{\Psi} = [\Psi_1, \Psi_2, \ldots, \Psi_m]$ is related to $1 + \lambda$ by

$$\mu_{\Gamma_i} = \sqrt{\frac{k\Psi_i}{k+1}} \tag{36}$$

Replacing this in (30), we have

$$1 + \lambda = \frac{1}{1+k} + \frac{k}{1+k}\left(\sum_{i=1}^{m} \sqrt{\Psi_i}\cos(2\pi\Gamma_i f)\right)^2 + \frac{k}{1+k}\left(\sum_{i=1}^{m} \sqrt{\Psi_i}\sin(2\pi\Gamma_i f)\right)^2 \tag{37}$$

It can be argued that, in most cases, the power of earlier taps are stronger than the later ones since later taps experience more delay and more attenuation (i.e. $\Psi_1 \geq \Psi_2 \geq \cdots \geq \Psi_m$). Therefore we can use Chebyshev's inequality and write

$$\left(\sum_{i=1}^{m} \sqrt{\Psi_i}\cos(2\pi\Gamma_i f)\right)^2 \geq \left(\sum_{i=1}^{m} \sqrt{\Psi_i}\right)^2 \left(\sum_{i=1}^{m} \cos(2\pi\Gamma_i f)\right)^2 \tag{38}$$

$$\left(\sum_{i=1}^{m} \sqrt{\Psi_i}\sin(2\pi\Gamma_i f)\right)^2 \geq \left(\sum_{i=1}^{m} \sqrt{\Psi_i}\right)^2 \left(\sum_{i=1}^{m} \sin(2\pi\Gamma_i f)\right)^2 \tag{39}$$

This lets us write a lower bound on (37) as

$$1 + \lambda \geq \frac{1}{1+k} + \frac{k}{1+k}\left(\sum_{i=1}^{m} \sqrt{\Psi_i}\right)^2 \times \left[\left(\sum_{i=1}^{m} \cos(2\pi\Gamma_i f)\right)^2 + \left(\sum_{i=1}^{m} \sin(2\pi\Gamma_i f)\right)^2\right] \tag{40}$$

Furthermore, since $0 \leq \Psi_i \leq 1$ for $\forall i$, we have

$$\left(\sum_{i=1}^{m} \sqrt{\Psi_i}\right)^2 \geq \sum_{i=1}^{m} \left(\sqrt{\Psi_i}\right)^2 = 1 \tag{41}$$

and (40) is further lower bounded as

$$1 + \lambda \geq \frac{1}{1+k} + \frac{k}{1+k} \times \left[\left(\sum_{i=1}^{m} \cos(2\pi\Gamma_i f)\right)^2 + \left(\sum_{i=1}^{m} \sin(2\pi\Gamma_i f)\right)^2\right] \tag{42}$$

where the equality holds if $\Psi_1 = \Psi_2 = \cdots = \Psi_m = 1/m$ (i.e. uniform PDP).

Assuming that taps are located at equal distances of r, the right-hand side of above inequality can be written as

$$1 + \lambda \geq \frac{1}{k+1} + \left(\frac{k}{m(k+1)}\right)\frac{1 - \cos(m2\pi rf)}{1 - \cos(2\pi rf)} \tag{43}$$

which yields the formula in (33) obtained under the assumption of uniform PDP in the previous section.

Our results indicate that uniform PDP results in the lowest capacity among different PDP types. Furthermore, it is observed from (37) that when more power is localised at a small number of taps, capacity increases and becomes closer to the capacity of frequency-flat channel where all of the power is localised at only one tap.

6 Numerical results

In this section, we present numerical results for the derived capacity expressions. Unless otherwise noted, we have the following assumptions: We consider a carrier frequency of 30 kHz and a transmission distance of $d = 1$ km. We assume temperature $T = 22°C$, depth $D = 50$ m, acidity of 8 pH, salinity $S = 35$ ppt, wind speed $\omega = 0$ m/s and spreading factor $s = 1.5$. We assume that the UWA channel experiences a multipath delay spread of 13 ms and has the order of $L = 130$. The number of significant delay taps is $m = 10$ and located at equal distances from each other with a uniform PDP, that is, the power of each significant tap is $1/m$. The Rician k factor for the significant taps is 2 dB.

Accuracy of derived expression and effect of ISI and distance: In Fig. 1, we present the capacity as a function of SNR for different link distances. As benchmarks, the capacity of AWGN and frequency-flat Rician fading channel are also depicted in this figure. In an effort to demonstrate the accuracy of derived expression for average channel capacity, we further plot the derived expression in (27) and compare it with the numerical evaluation of (21). In the calculation of (27), first hundred terms of the series are considered. It is observed from Fig. 1 that the derived expression coincides perfectly with numerical results.

Comparison with frequency-flat case under the assumptions of same coloured noise and path loss reveals that the presence of ISI reduces the capacity. Specifically, at SNR = 20 dB, a capacity of 3.19 bit/s/Hz is achieved for $d = 1$ km over frequency-flat Rician fading channel. This reduces to 2.78 bit/s/Hz over frequency-selective channel for the same link distance. It is further observed that an increase in distance would result in a decrease in capacity as expected. Specifically, at SNR = 20 dB, a capacity of 2.78 bit/s/Hz is achieved for $d = 1$ km. This reduces to 2.45 bit/s/Hz for $d = 2$ km. It further reduces to 2.07 and 1.75 bit/s/Hz, respectively, for $d = 3$ and 4 km.

Effect of taps' locations: In Fig. 2, we investigate the effect of significant channel taps' locations on the capacity. We assume ten significant taps (i.e. $m = 10$) with uniform PDP and consider the following $\boldsymbol{\Gamma}$ vectors to indicate the location of significant taps:

- $\boldsymbol{\Gamma}_1 = [1, 2, 3, 4, 5, 6, 7, 8, 9, 10]$ (i.e. the locations of significant taps are consecutive).
- $\boldsymbol{\Gamma}_2 = [1, 2, 3, 4, 5, 6, 7, 8, 11, 20]$.
- $\boldsymbol{\Gamma}_3 = [1, 2, 3, 4, 5, 6, 11, 20, 47, 128]$.
- $\boldsymbol{\Gamma}_4 = [1, 15, 29, 43, 57, 71, 85, 99, 113, 127]$, (i.e. equally spaced taps).

doi: 10.1049/iet-com.2014.0083

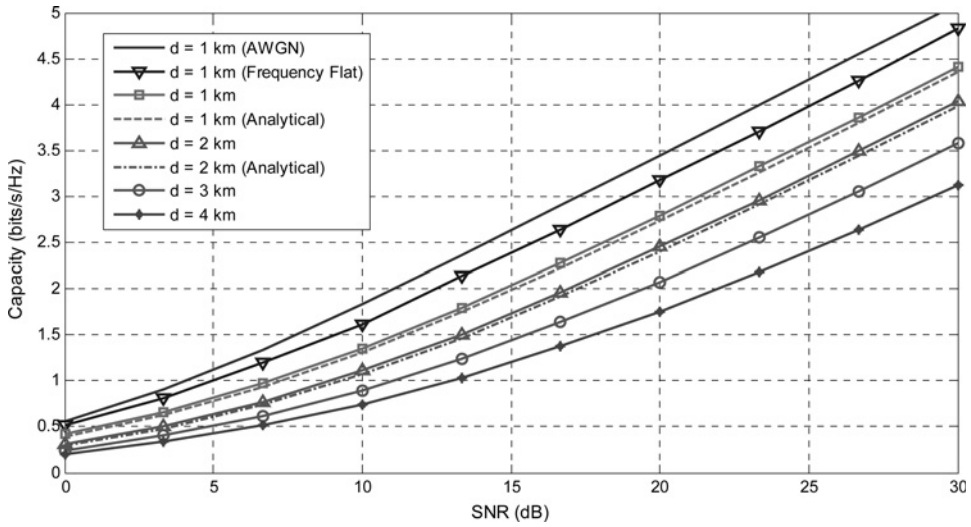

Fig. 1 *Capacity as a function of SNR for different link distances*

It is observed from Fig. 2 that as the spacing between significant taps increases, capacity becomes closer to the capacity of frequency-flat channel. For example, in a channel with $\mathbf{\Gamma}_1$, a capacity of 1.27 bit/s/Hz is achieved at SNR = 10 dB. This climbs up to 1.49 bit/s/Hz for a channel with $\mathbf{\Gamma}_3$, where the spacing between the significant taps is more. This further increases to 1.54 bit/s/Hz for $\mathbf{\Gamma}_4$ which corresponds to the case of equal spacing. These observations further confirm the concluding remarks of Section 5.1 which states that capacity increases as the spacing between significant taps (r) increases. Specifically, in a channel with $\mathbf{\Gamma}_1$ with $r = 1$, the lowest capacity is achieved. On the other hand, for the case of $\mathbf{\Gamma}_4$ with $r = 14$, the capacity increases and becomes closer to the capacity of frequency-flat channel.

Effect of PDP: In Fig. 3, we study the effect of significant channel taps' PDP on the capacity. Assuming $m = 10$, we consider the following PDPs:

- $\mathbf{\Psi}_1 = [1]$ (i.e. frequency-flat Rician fading channel).
- $\mathbf{\Psi}_2 = [0.7, 0.1, 0.025, 0.025, 0.025, 0.025, 0.025, 0.025, 0.025, 0.025]$.
- $\mathbf{\Psi}_3 = [0.5, 0.1, 0.05, 0.05, 0.05, 0.05, 0.05, 0.05, 0.05, 0.05]$.
- $\mathbf{\Psi}_4 = [0.1, 0.1, 0.1, 0.1, 0.1, 0.1, 0.1, 0.1, 0.1, 0.1]$ (i.e. uniform PDP).

Our results demonstrate that uniform PDP results in the lowest capacity among the considered PDPs. This confirms our observations in Section 5.2 which states that under the assumption of equally spaced taps, uniform PDP results in lowest capacity as $\mathbf{\Psi}_4$ does in Fig. 3. It is also observed that when more power is localised at a small number of taps (compare $\mathbf{\Psi}_3$, $\mathbf{\Psi}_2$) capacity increases and becomes closer to the capacity of frequency-flat channel (i.e. $\mathbf{\Psi}_1$) as discussed in Section 5.2.

Effect of the number of significant channel taps: In Fig. 4, we examine the effect of the number of significant channel taps on the capacity. We consider $m = 2$, 4, 6, 8, 10 and 20 and assume that significant taps are located at equal

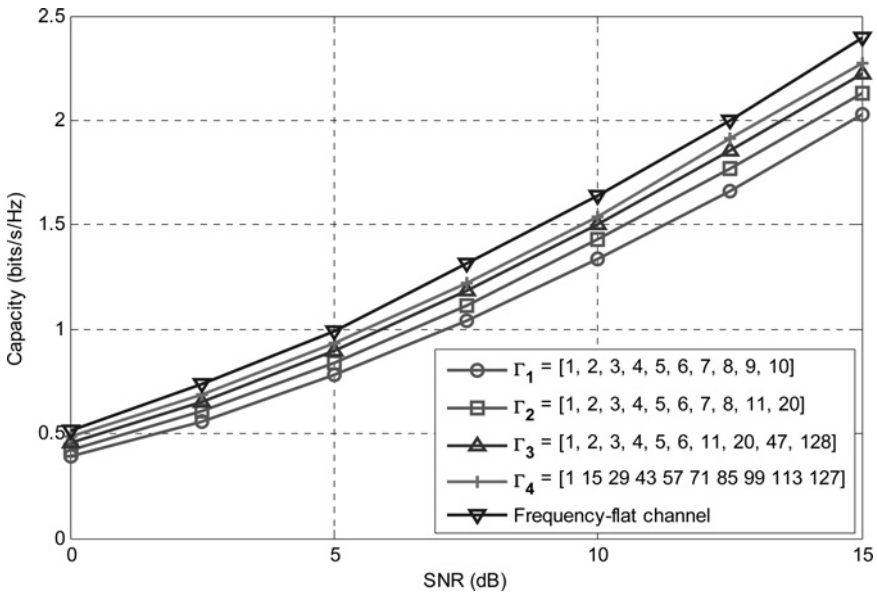

Fig. 2 *Capacity against SNR for different locations of significant taps (d = 1 km)*

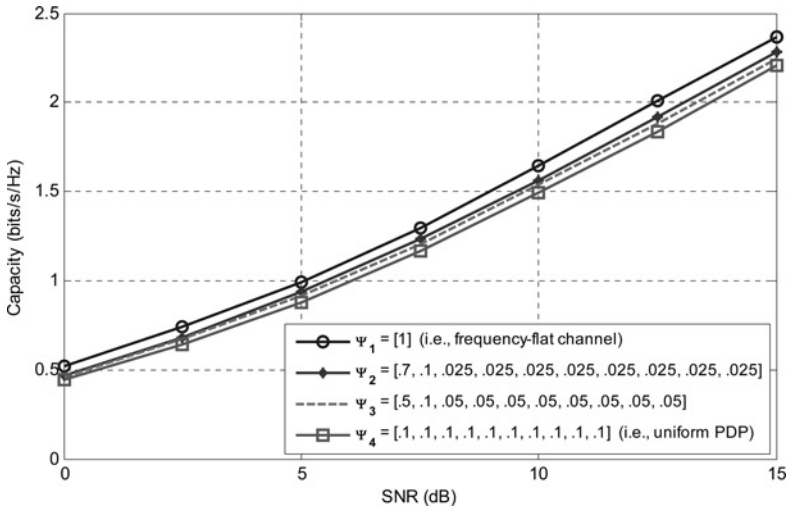

Fig. 3 *Effect of PDP of significant taps on the capacity (d = 1 km)*

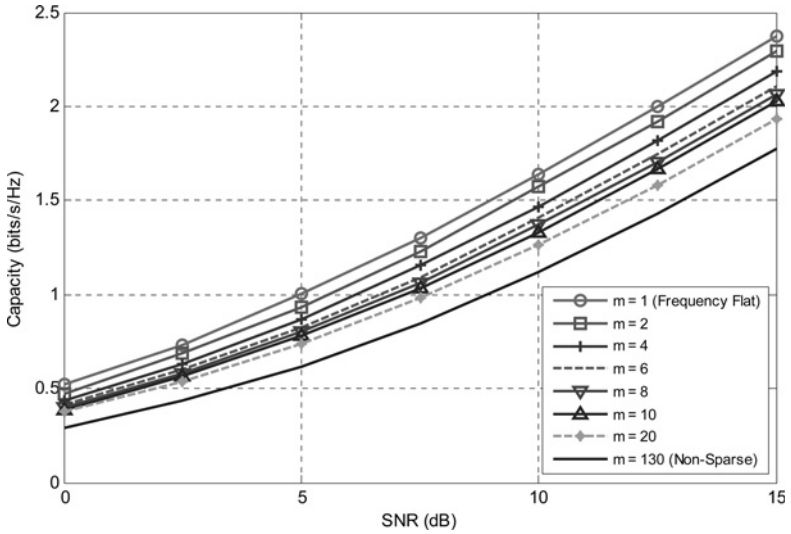

Fig. 4 *Capacity against SNR for different numbers of significant taps (d = 1 km)*

distances from each other with a uniform PDP. As limiting cases, we also include the case of $m = 1$ (i.e. frequency-flat channel) and $m = L = 130$ (i.e. non-sparse channel). It is observed that as the number of significant taps increases and the total power is spread over many taps, capacity decreases. This is expected as discussed in Section 5. Particularly, it can be checked from (33) that when m increases, the term $1 + \lambda$ decreases and, consequently, the capacity also decreases.

Effect of wind speed: In Fig. 5, we examine the capacity for wind speeds of 0, 1 and 2 m/s. The highest capacity among these three cases is achieved when the wind speed is zero. Specifically, a capacity of 2.77 bit/s/Hz is achieved for $\omega =$ 0 m/s and $d = 1$ km. This reduces to 1.76 bit/s/Hz for $\omega = 1$ m/s and further reduces to 1.37 bit/s/Hz for $\omega = 2$.

7 Capacity optimisation

In this section, we aim to determine carrier frequency, input signal PSD and bandwidth as to optimise the capacity.

7.1 Choice of optimal frequency

Maximisation of the channel capacity in (21) with respect to carrier frequency is equivalent to maximising $G(f, d)/Z_w(f)$. Recalling the definition of the path gain and differentiating the resulting expression with respect to f and setting it to zero, we have

$$d\frac{\partial a(f)_{\mathrm{dB}}}{\partial f} + \frac{\partial Z_w(f)_{\mathrm{dB}}}{\partial f} = 0 \tag{44}$$

After some mathematical manipulations (see Appendix), we find the optimal frequency as (see (45))

where S, D and T represent the salinity, depth and temperature, respectively.

The optimal frequency as a function of transmission distance is illustrated in Fig. 6 for different values of temperature, depth and salinity. It is also observed that direct numerical solution of (44) and the derived approximate closed-form solution in (45) provide a perfect

$$f_{\mathrm{opt}} \cong \sqrt{\frac{367.5}{S/35(1 + (T/43))\exp(-(D/6) - (T/17))d - 0.28\exp(-2T/17)}} \tag{45}$$

doi: 10.1049/iet-com.2014.0083

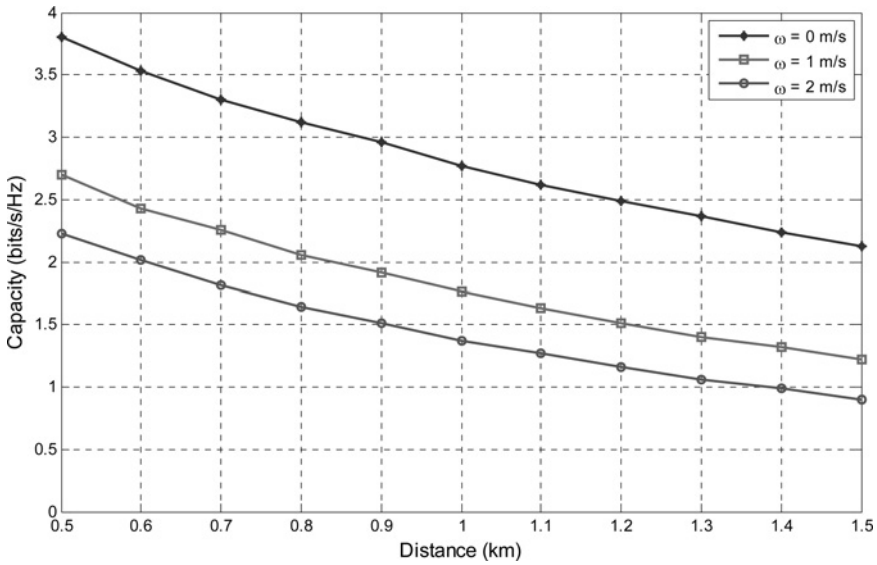

Fig. 5 *Capacity against distance for different wind speeds (SNR = 20 dB)*

match. Assuming temperature of 22°C, depth of 50 m and salinity of 35 ppt, the optimal frequencies are found to be 55, 30, 21.37 and 17.17 kHz, respectively, for distances of $d = 350$ m, 1 km, 2 km and 3 km. This indicates that the optimal frequency decreases with increasing transmission distance.

Furthermore, we consider four cases to demonstrate the effect of temperature, depth and salinity on the optimal frequency. It is observed from Fig. 6 that an increase in temperature and/or depth results in an increase in optimal frequency, whereas an increase in salinity results in a decrease in optimal frequency. For example, at 22°C, depth of 50 m and salinity of 35 ppt, the optimal frequency is 30 kHz for $d = 1$ km. Keeping temperature and salinity fixed and changing the depth from 50 m to 2 km, the optimal frequency increases from 30 to 37 kHz. Keeping temperature and depth fixed and changing the salinity from 30 to 35 ppt, the optimal frequency reduces from 40 to 37 kHz. On the other hand, keeping depth and salinity fixed and changing the temperature from 15 to 22°C, the optimal frequency increases from 25 to 30 kHz.

7.2 Optimal power allocation

If the CSI is present at both transmitter and receiver side, we can maximise the capacity with respect to the PSD of input signal. A direct maximisation of (20) appears to be intractable to compute. By equivalency of (19) and (20), we reconsider the power allocation problem in the continuous frequency domain via a finite dimension domain. We then take the limit as $N \to \infty$ to obtain the desired result. Let C_n be the capacity for one realisation of the channel and assume that n belongs to time interval [0, T]. For each sub-channel, we define $\beta_n(f_i) = Z_w(f_i)/(G(f_i,d)/h_n(f_i)|^2)$. We first maximise C_n with respect to input PSD $P_n(f_i)$, then we average over all realisations of fading states [30]. The objective function C_n is given by

$$C_n = \lim_{N\to\infty} \frac{1}{2N} \sum_{i=1}^{N} \log\left(1 + \frac{P_n(f_i)}{\beta_n(f_i)}\right) \tag{46}$$

The solution involves a combination of water-filling over

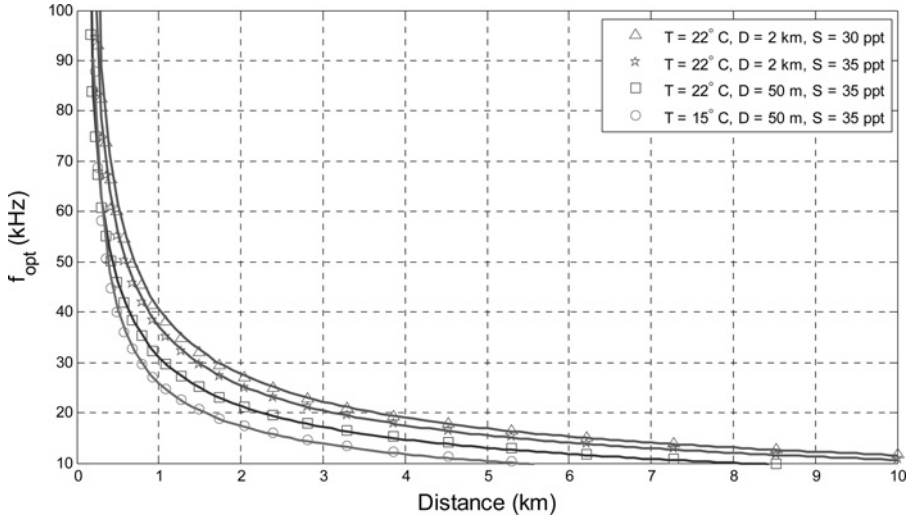

Fig. 6 *Optimal carrier frequency f_{opt} in terms of environmental parameters*
Solid lines indicate the approximation formula given by (45)

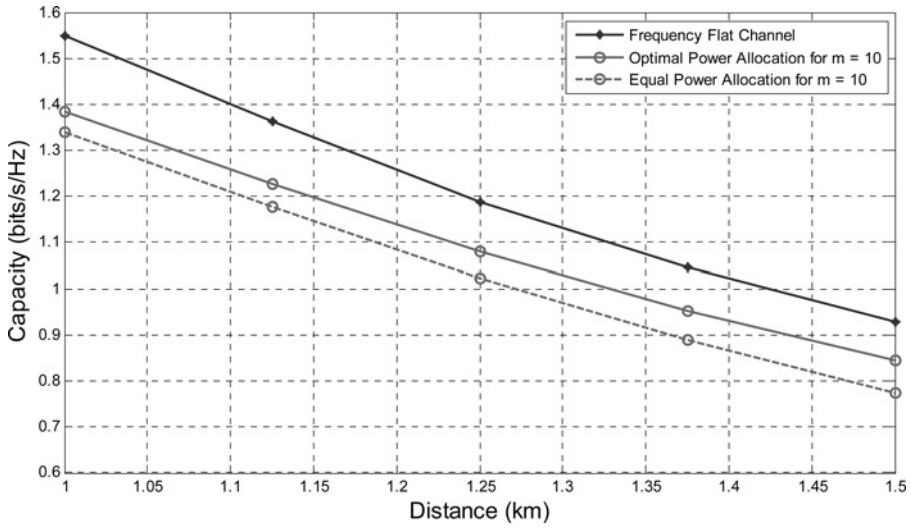

Fig. 7 *Capacity against distance for optimal and equal power allocation of input PSD (SNR = 10 dB)*

frequency and time, that is

$$P_{n,\text{opt}}(f_i) = [v_n - \beta_n(f_i)]^+ \tag{47}$$

In the limit of $N \to \infty$, as the number of sub-bands N grows, the width of sub-bands goes to zero and the optimal power allocation converges to

$$P_{n,\text{opt}}(f) = [v_n - \beta_n(f)]^+ \tag{48}$$

where v_n is the power price chosen to satisfy the power constraint for the nth realisation of the channel. Considering a bandwidth W, we can write

$$\frac{1}{W}\int_W [v_n - \beta_n(f)]^+ \, \mathrm{d}f = P_t \tag{49}$$

Fig. 7 depicts results for equal and optimal power allocation. For $d = 1.5$ km, a capacity of 0.77 bit/s/Hz is achieved for equal power allocation. This increases to 0.84 bit/s/Hz for optimal power allocation.

7.3 Optimal bandwidth

It is possible to further optimise the capacity in (21) with respect to bandwidth. To compare the capacities with different bandwidths in a fair way, neither a pre-specified SNR nor a fixed transmit power is applicable in our case. Since, in UWA communication under consideration, SNR is dependent on the operating frequency band (because of frequency dependency of ambient noise and path loss), and therefore to achieve a fixed SNR, either an increase in bandwidth or an increase in transmission power is needed. In both cases, this results in an increase of the total energy of the signal. Similarly, a fixed transmission power P_t is not fair since the larger bandwidths will result in larger capacity as the total energy of the signal (i.e. $P_t W$) increases. Here, we make our comparisons under the assumption of fixed total energy of the signal, that is, $E_s = P_t W$ and find the optimal bandwidth.

To optimise the capacity with respect to bandwidth, we can adopt two different approaches:

- finding the optimal bandwidth for each realisation of the channel and
- finding a single optimal bandwidth for the average capacity.

Here, we investigate the second approach which is also of more practical values since most communication systems typically work in a predefined bandwidth region.

The capacity of the Gaussian channel is a concave function of P_t [31], therefore under the assumption of fixed value for E_s, it is also a concave function of W. The optimum value of W, that is, W_{opt}, can be found by iterative methods. The optimised C_n can be then written as

$$C_n = \frac{1}{2}\int_{W_{\text{opt}}} \log\left(1 + \frac{[v_n - \beta_n(f)]^+}{\beta_n(f)}\right) \mathrm{d}f \tag{50}$$

The optimal input PSD has a water-filling type structure over both frequency and time and shows a 'floating' effect since it changes with respect to time. To capture the effect of fading, we need to average C_n over time interval $[0, T]$ which is given by $(1/T)\sum_{n=1}^{T} C_n$. As $T \to \infty$ this quantity converges to the expectation by the law of large numbers and can be expressed as

$$C = E_{|h(f)|^2}\left[\frac{1}{2}\int_{W_{\text{opt}}} \log\left(1 + \frac{[v - \beta(f)]^+}{\beta(f)}\right) \mathrm{d}f\right] \tag{51}$$

In the following, we assume $d = 350$ m, $T = 22°$C, $D = 50$ m, $S = 35$ ppt and use the corresponding optimal carrier frequency (i.e. $f_{\text{opt}} = 55$ kHz). In Table 1, the optimal bandwidth W_{opt} is presented for optimal and equal power allocation.

In Fig. 8, the capacity in bit/s against different bandwidths is depicted assuming $E_s = 50$, 55 and 60 dB. As we expect from Table 1, the optimised capacity (with respect to bandwidth) takes place at $W_{\text{opt}} = 32$, 43 and 55 kHz, respectively, for $E_s = 50$, 55 and 60 dB under the assumption of equal power allocation. This is readily confirmed from Fig. 8. The corresponding capacity values are 2.65, 6.85 and 16.21 kbit/s.

Optimum power allocation along with optimised bandwidth will further increase the capacity. From Fig. 8,

doi: 10.1049/iet-com.2014.0083

Table 1 Optimal bandwidths obtained for different values of E_s

	E_s (dB)	10	15	20	25	30	35	40	45	50	55	60	65	70
W_{opt}, kHz	optimal power allocation (CSI)	7	10	13	17	22	28	35	44	52	60	68	78	88
	equal power allocation (no. CSI)	2	3	4	5	8	12	17	23	32	43	55	69	82

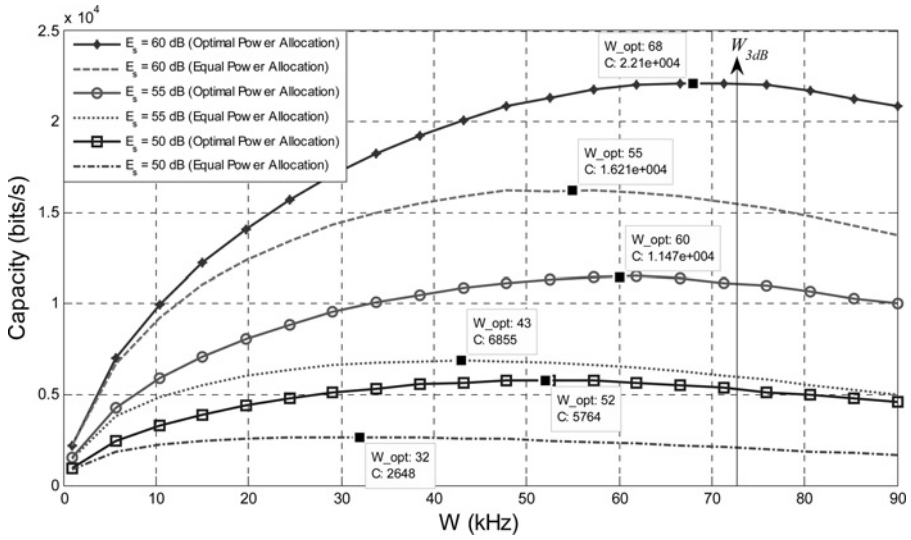

Fig. 8 *Capacity against different values of bandwidth (d = 350 m)*

we observe that the capacity climbs up to 5.76, 11.47 and 22.11 kbit/s, respectively, for $E_s = 50$, 55 and 60 dB in the case of optimal power allocation. It should be noted that optimal power allocation does not help for the bandwidths larger than the optimal bandwidth. In these cases, capacity remains approximately constant in comparison with the capacity obtained under optimal bandwidth. Since water-filling prevents the use of excessive bandwidth, increasing the bandwidth is useless. In equal power allocation, when the bandwidth is larger than the optimal bandwidth, capacity is much reduced in comparison to the capacity obtained under optimal bandwidth. The reason is that we allocate the power all over the available bandwidth and energy is now wasted in parts of the channel that should have been turned off because of the low channel quality.

8 Conclusions

We have investigated the information theoretical performance analysis and optimisation of point-to-point UWA systems. We have assumed a single-carrier communication architecture and sparse Rician frequency-selective UWA channel with ISI. We have considered non-white Gaussian distribution to model the ambient noise and taken into account the effects of environmental parameters such as temperature, salinity, pressure as well as distance and frequency. We have developed an equivalent channel model for UWA channel with ISI under consideration and shown that the capacity of the equivalent channel converges to that of the operating channel in the limit of infinite block length. Using these results, we have first obtained a capacity expression for the UWA channel and demonstrated the dependency of capacity on channel parameters (e.g. the number, location and PDP of significant taps) and environmental parameters (e.g. temperature, salinity and pressure). Then, we have used this expression to determine the optimal carrier frequency, input signalling and bandwidth.

9 Acknowledgments

This work was supported by the Turkish Scientific and Research Council (TUBITAK) under grant 110E092. This paper was presented in part at the IEEE EUROCON Conference, Zagreb, Croatia, July 2013.

10 References

1 Vasilescu, I., Kotay, K., Rus, D., Corke, P., Dunbabin, M.: 'Data collection, storage and retrieval with an underwater optical and acoustical sensor network'. Proc. Sensys, ACM, 2005, pp. 154–165
2 Stojanovic, M.: 'Underwater wireless communications: current achievements and research challenges'. IEEE Oceanic Engineering Society Newsletter, Spring, 2006
3 Akyildiz, I.F., Pompili, D., Melodia, T.: 'State of the art in protocol research for underwater acoustic sensor networks'. ACM Mobile Computing and Communication Review, ACM, October 2007
4 Smith, R.N., Chao, Y., Li, P.P., Caron, D.A., Jones, B.H., Sukhatme, G. S.: 'Planning and implementing trajectories for autonomous underwater vehicles to track evolving ocean processes based on predictions from a regional ocean model', *Int. J. Robot. Res.*, 2010, **29**, (12), pp. 1475–1497
5 Chen, K., Ma, M., Cheng, E., Yuan, F., Su, W.: 'A survey on MAC protocols for underwater wireless sensor networks', *IEEE Commun. Surv. Tutor.*, 2014, **16**, (3), pp. 1433–1447
6 Erol-Kantarci, M., Mouftah, H.T., Oktug, S.: 'A survey of architectures and localization techniques for underwater acoustic sensor networks', *IEEE Commun. Surv. Tutor.*, 2011, **13**, (3), pp. 487–502
7 Hollinger, G., Yerramalli, S., Singh, S., Mitra, U., Sukhatme, G.S.: 'Distributed coordination and data fusion for underwater search'. Proc. IEEE Conf. Robotics and Automation, 2011, pp. 349–355
8 Gkikopouli, A., Nikolakopoulos, G., Manesis, S.: 'A survey on underwater wireless sensor networks and applications'. 20th Mediterranean Conf. Control & Automation (MED), Barcelona, Spain, July 2012, pp. 1147–1154
9 Headrick, R., Freitag, L.: 'Growth of underwater communication technology in the US Navy', *IEEE Commun. Mag.*, 2009, **47**, (1), pp. 80–82

10 Stojanovic, M., Preisig, J.: 'Underwater acoustic communication channels: propagation models and statistical characterization', *IEEE Commun. Mag.*, 2009, **47**, (1), pp. 84–89
11 Tse, D.: Capacity of wireless channels in Viswanath, P. (Ed.): 'Fundamentals of wireless communication' (Cambridge University Press, New York, NY, 2005), pp. 166–227
12 Stojanovic, M.: 'On the relationship between capacity and distance in an underwater acoustic communication channel', *ACM SIGMOBILE Mob. Comput. Commun. Rev.*, 2007, **11**, (4), pp. 34–43
13 Choudhuri, C., Mitra, U.: 'Capacity bounds and power allocation for underwater acoustic relay channels with ISI'. Proc. Fourth ACM Int. Workshop on UnderWater Networks, ACM, November 2009, p. 6
14 Polprasert, C., Ritcey, J.A., Stojanovic, M.: 'Capacity of OFDM systems over fading underwater acoustic channels', *IEEE J. Ocean. Eng.*, 2011, **36**, (4), pp. 514–524
15 Kwon, H., Birdsall, T.: 'Channel capacity in bits per joule', *IEEE J. Ocean. Eng.*, 1986, **11**, (1), pp. 97–99
16 Leinhos, H.A.: 'Capacity calculations for rapidly fading communications channels', *IEEE J. Ocean. Eng.*, 1996, **21**, (2), pp. 137–142
17 Socheleau, F.X., Stojanovic, M., Laot, C., Passerieux, J.M.: 'Information-theoretic analysis of underwater acoustic OFDM systems in highly dispersive channels', *J. Electr. Comput. Eng.*, 2012, doi: 10.1155/2012/716720
18 Brekhovskikh, L.M., Lysanov, I.P.: 'Fundamentals of ocean acoustics' (Springer, New York, 2003)
19 Coates, R.F.: 'Underwater acoustic systems' (J. Wiley, 1989)
20 Francois, R.E., Garrison, G.R.: 'Sound absorption based on ocean measurements. Part I: pure water and magnesium sulfate contributions', *J. Acoust. Soc. Am.*, 1982, **72**, p. 896
21 Francois, R.E., Garrison, G.R.: 'Sound absorption based on ocean measurements. Part II: boric acid contribution and equation for total absorption', *J. Acoust. Soc. Am.*, 1982, **72**, (6), pp. 1879–1890
22 Hirt, W., Massey, J.L.: 'Capacity of the discrete-time Gaussian channel with intersymbol interference', *IEEE Trans. Inf. Theory*, 1988, **34**, (3), pp. 38–38
23 Al-Dharrab, S., Uysal, M.: 'Information theoretic performance of cooperative underwater acoustic communications'. 2011 IEEE 22nd Int. Symp. Personal Indoor and Mobile Radio Communications (PIMRC), September 2011, pp. 1562–1566
24 Proakis, J.G.: 'Digital communications' (McGraw-Hill, 1995)
25 Radosevic, A., Proakis, J.G., Stojanovic, M.: 'Statistical characterization and capacity of shallow water acoustic channels'. Proc. IEEE OCEANS 2009-EUROPE, May 2009
26 Goldsmith, A.J., Effros, M.: 'The capacity region of broadcast channels with intersymbol interference and colored Gaussian noise', *IEEE Trans. Inf. Theory*, 2001, **47**, (1), pp. 219–240
27 Cover, T.M., Thomas, J.A.: 'Elements of information theory' (John Wiley & Sons, 2012)
28 Simon, M.K., Alouini, M.S.: 'Digital communication over fading channels' (Wiley.com, 2005), vol. 95
29 Lee, W.C.: 'Estimate of channel capacity in Rayleigh fading environment', *IEEE Trans. Veh. Technol.*, 1990, **39**, (3), pp. 187–189
30 Gallager, R.G.: 'An inequality on the capacity region of multiaccess multipath channels' (Springer US, 1994), pp. 129–139
31 Chen, H.W., Yanagi, K.: 'The convex-concave characteristics of Gaussian channel capacity functions', *IEEE Trans. Inf. Theory*, 2006, **52**, (5), pp. 2167–2172
32 Ainslie, M.A., McColm, J.G.: 'A simplified formula for viscous and chemical absorption in sea water', *J. Acoust. Soc. Am.*, 1998, **103**, (3), pp. 1671–1672

11 Appendix

11.1 Derivation of optimal carrier frequency

To derive the optimal frequency, we begin with (44). For $10 \le f \le 100$ kHz, we can approximate $\partial Z_w(f)_{\mathrm{dB}}/\partial f$ by

$$\frac{\partial Z_w(f)_{\mathrm{dB}}}{\partial f} \cong \frac{-20}{\ln(10)}\frac{1}{f} \tag{52}$$

Recall that $a(f)_{\mathrm{dB}}$ is given by (1). Let us define $M_1 = (A_1B_1C_1f^2)/\left(C_1^2+f^2\right)$, $M_2 = (A_2B_2C_2f^2)/\left(C_2^2+f^2\right)$ and $M_3 = A_3B_3f^2$. In the frequency range under consideration, we can safely assume $M_1 \cong 0$, $M_3 \cong 0$, since M_2 (involving $MgSO_4$ contributions) dominates the others [20]. Therefore we have

$$\frac{\partial a(f)_{\mathrm{dB}}}{\partial f} \cong \frac{2A_2B_2C_2^3f}{\left(C_2^2+f^2\right)^4} \tag{53}$$

Replacing (52) and (53) in (44) and defining $\alpha = 10/d\ \ln(10)$, we obtain

$$\alpha f^4 + \left(2\alpha C_2^2 - A_2B_2C_2^3\right)f^2 + \alpha C_2^4 = 0 \tag{54}$$

which is a quadratic equation. Within $10 \le f \le 100$ kHz and under the assumptions of $-2° \le T \le 22°$, $S = 30$–35 ppt and $D \le 3.5$ km [20], we have $C_2^4 \gg f^4$. Therefore we can approximate (54) by $\left(2\alpha C_2^2 - A_2B_2C_2^3\right)f^2 + \alpha C_2^4 = 0$ where the approximated solution is given by

$$f = C_2\sqrt{\frac{\alpha}{A_2B_2C_2 - 2\alpha}} \tag{55}$$

Noting $A_2B_2 = 0.52(1 + T/43)(S/35)\mathrm{e}^{-D/6}$ and $C_2 = f_2 = 42\mathrm{e}^{(T/17)}$ [32], the optimal frequency can be found as (see (56))

$$f \cong \sqrt{\frac{367.5}{S/35(1+(T/43))\exp(-(D/6)-(T/17))d - 0.28\ \exp(-2T/17)}} \tag{56}$$

doi: 10.1049/iet-com.2014.0083